HHS Public Access

Author manuscript

Science. Author manuscript; available in PMC 2022 July 16.

Published in final edited form as:

Science. 2021 July 16; 373(6552): 337–342. doi:10.1126/science.abf2155.

Wafer-scale heterostructured piezoelectric bio-organic thin films

Fan Yang[1,2,3,†], **Jun Li**[1,†], **Yin Long**[1], **Ziyi Zhang**[1], **Linfeng Wang**[1], **Jiajie Sui**[1], **Yutao Dong**[1], **Yizhan Wang**[1], **Rachel Taylor**[4], **Dalong Ni**[5], **Weibo Cai**[5], **Ping Wang**[2,3], **Timothy Hacker**[4], **Xudong Wang**[1,*]

[1]Department of Materials Science and Engineering, University of Wisconsin–Madison, Madison, WI 53706, USA.

[2]School of Civil Engineering, Southwest Jiaotong University, Chengdu 610031, China.

[3]Key Laboratory of High-speed Railway Engineering, Ministry of Education, Chengdu 610031, China.

[4]Cardiovascular Research Center, University of Wisconsin–Madison, Madison, WI 53705, USA.

[5]Department of Radiology and Medical Physics, University of Wisconsin–Madison, Madison, WI 53705, USA.

Abstract

Piezoelectric biomaterials are intrinsically suitable for coupling mechanical and electrical energy in biological systems to achieve in vivo real-time sensing, actuation, and electricity generation. However, the inability to synthesize and align the piezoelectric phase at a large scale remains a roadblock toward practical applications. We present a wafer-scale approach to creating piezoelectric biomaterial thin films based on γ-glycine crystals. The thin film has a sandwich structure, where a crystalline glycine layer self-assembles and automatically aligns between two polyvinyl alcohol (PVA) thin films. The heterostructured glycine-PVA films exhibit piezoelectric coefficients of 5.3 picocoulombs per newton or 157.5×10^{-3} volt meters per newton and nearly an order of magnitude enhancement of the mechanical flexibility compared with pure glycine crystals. With its natural compatibility and degradability in physiological environments, glycine-PVA films may enable the development of transient implantable electromechanical devices.

*Corresponding author. xudong.wang@wisc.edu.
†These authors contributed equally to this work.

Author contributions: F.Y., J.L., and X.W. conceived the idea and designed the research. F.Y., J.S., and J.L. performed film synthesis and device fabrication. F.Y., J.L., and J.S. carried out mechanical and piezoelectric characterizations. L.W. conducted DFT calculations. J.L., Z.Z., Y.D., and Y.W. performed morphology and structure characterizations. F.Y. and Y.L. performed the in vitro biodegradation. J.L., Y.L., and D.N. conducted the cell toxicity study. R.T. and T.H. performed the in vivo experiments. F.Y., J.L., and X.W. analyzed the data and wrote the manuscript. All authors reviewed and commented on the manuscript.

Competing interests: F.Y., J.L., and X.W. are inventors on a patent application [P210089US01(1512.777)] filed through the Wisconsin Alumni Research Foundation.

SUPPLEMENTARY MATERIALS

science.sciencemag.org/content/373/6552/337/suppl/DC1

Materials and Methods
Supplementary Text
Figs. S1 to S30
Table S1
References (31–41)
Movies S1 to S4

Piezoelectricity is a material property that couples mechanical energy with electricity. It is also a relatively common phenomenon that can be found in many biological systems (1–3). More than a century of research on piezoelectric materials has led to advancements in inorganic piezoelectric crystals in terms of processing techniques, property enhancement, and multifunctionality. This group of materials is used in a broad range of electromechanical systems for sensing, acoustics, imaging, actuation, and energy harvesting (4–8). For use in biotechnology, these materials must also show flexibility, biocompatibility, and biodegradability (9, 10). Unfortunately, inorganic piezoelectric materials are intrinsically rigid, brittle, and challenging to process and may contain toxic elements. Even synthetic piezoelectric polymers, such as polyvinylidene difluoride (PVDF), are not able to satisfy many requirements, particularly those for flexibility and degradability.

Piezoelectric biomaterials—for example, silk (11, 12), collagen (13, 14), amino acids (15, 16), chitin (17), cellulose (18), and viral particles (19)—can naturally offer many potentially beneficial properties of biomaterials such as reliability, biocompatibility, reproducibility, and flexibility. They are mostly biodegradable, and their production is considered environmentally sustainable. However, because of the lack of large-scale assembly and domain aligning, studies of their piezoelectricity are still primarily at the conceptual level. Within this intriguing group of piezoelectric biomaterials, glycine, the simplest amino acid, stands out with a high piezoelectric coefficient (d_{33} up to 10 pC/N) and exceptional stability (γ-glycine) (20). Nevertheless, similar to many inorganic molecules, pure glycine tends to form fragile bulk crystals with a very high Young's modulus (~30 GPa). Moreover, glycine requires an extremely high electric field (more than GV/m) to align the domains, which makes it rather challenging for its polycrystalline film to exhibit macroscopic piezoelectricity.

We report a self-assembly strategy for wafer-scale synthesis of heterostructured piezoelectric glycine thin films. The films have a polyvinyl alcohol (PVA)–glycine-PVA sandwich structure, where the hydrogen bonding between PVA and glycine at the interface leads to the formation and self-alignment of γ-glycine crystals across the entire film. The as-synthesized film exhibits a superb, stable, and uniform piezoelectric property, as well as excellent flexibility and biocompatibility.

Glycine-PVA films were synthesized by direct solidification from their mixture solution at 60°C (Fig. 1A; detailed synthesis procedures are included in the materials and methods section of the supplementary materials). Because of the low surface tension, the solution evenly dispersed on the supporting surface, forming a uniform liquid film. As the solvent evaporated, the liquid film crystalized from the edges and expanded rapidly across the entire area within 30 min (movie S1). Through this approach, the solidified film could reach a fairly large area, which was only limited by the size of the supporting surface. The film could be directly peeled off from the surface, exhibiting excellent uniformity, integrity, and flexibility (inset of Fig. 1A and movie S2). A cross-sectional scanning electron microscopy (SEM) image revealed that the as-received film had a three-layer structure with an overall thickness of ~30 μm (Fig. 1B). The top and bottom layers had the same thickness (~7 μm), which was less than that of the middle layer (~16 μm), where clear crystalline features could be observed. Corresponding energy-dispersive x-ray spectroscopy (EDS) mapping

showed that the nitrogen element (only from glycine) was concentrated in the middle layer region (Fig. 1C), whereas the carbon element was more distributed at the top and bottom shells (fig. S1), indicating that the middle layer was glycine and the top and bottom layers were primarily PVA. The crystalline domain of glycine exhibited a columnar geometry following the growth direction with an average width of ~230 μm and lengths extending to the centimeter scale (fig. S2). X-ray diffraction (XRD) spectra obtained from as-received films exhibited characteristic peaks (at 21.8° and 25.3°) of γ-phase glycine (red curve in Fig. 1D), and no diffraction peaks from other phases could be observed, confirming that the as-received film was dominated by the piezoelectric γ-glycine crystals. The very broad and low-intensity peak centered at 19.7° belongs to PVA, indicating its extremely low crystallinity. Without introducing PVA, the same procedure only yielded glycine crystals dominated by the nonpiezoelectric α phase (black curve in Fig. 1D).

Density function theory (DFT) was used to investigate the interactions between γ-glycine and PVA. Three possible alignment conditions that enable glycine molecules to bind with PVA chains are shown in Fig. 1E. DFT calculations revealed that when a glycine molecule has its two O atoms bound with the hydroxyl groups (–OH) on PVA chains, the overall system energy reached the minimum (Fig. 1F). Because PVA always has its –OH groups exposed, it could guide the packing of glycine molecules macroscopically and thus direct the nucleation and growth of the γ phase throughout the entire film. Without PVA to balance the dipole in glycine, the dipole direction in glycine molecules would exhibit an alternating distribution to minimize the internal electro-static energy, and the α phase would dominate (fig. S3).

The sandwiched heterostructure with continuous and uniform PVA outer layers was thus considered essential for the formation of piezoelectric γ-glycine film. Evolution of the heterostructure was attributed to the sequential precipitation of these two components from the mixture solution. As depicted in Fig. 1G, when water was evaporating, the less soluble PVA precipitated out first and accumulated at the interfaces owing to its amphiphilic nature (21, 22). As the concentration continuously rose, salting out of PVA would be activated at a certain point because of the competition for water hydration between the polymer and electrolyte molecules (glycine). Most of the PVA would precipitate out at both water-air and water-solid interfaces, leaving a glycine-rich solution in between. Further evaporation of water from the top surface would super-saturate the solution, yielding a concentration gradient from the top inner surface to the bulk solution. Glycine nucleated at the top inner surface near the liquid edge, where water evaporated the fastest owing to the positive surface curvature (fig. S4). As predicted by DFT, driven by the –OH groups on the PVA layer, the nuclei would preferably be the γ phase with their (001) facets facing the PVA layer (inset of Fig. 1G). These nuclei then quickly grew into the concentrated liquid confined in between the PVA layers and completely crystalized into a solid crystalline film with its phase and orientation defined by the nuclei. This process was visualized by a series of photographs recorded at different time points (figs. S5 and S6 and movie S3). It was further validated by terminating the film crystallization halfway and draining the remaining liquid (fig. S7). From the as-received thin film, three distinct regions could be observed. Cross-sectional SEM images revealed that the crystallized region had a normal sandwich structure, whereas the transparent amorphous region exhibited a uniform feature with a much smaller thickness.

A clear transition from the sandwich structure to the homogeneous layer could be observed in the center region with a sharp cutoff of the middle layer, which was confirmed to be glycine by EDS N-mapping.

This sandwiched heterostructure could be formed within a wide range of glycine-to-PVA ratio (0.5:1 to 5:1) (fig. S8). The thicknesses of the glycine and PVA layers and their ratio are directly related to their amounts in the solution mixture (fig. S9). All of the as-received thin films exhibited a pure γ-glycine XRD pattern without any observable peaks from other phases (fig. S10). This series of XRD patterns also revealed that the dominant out-of-plane orientation of the glycine films evolved from [110] to [101] as the glycine-to-PVA ratio increased from 0.5:1 to 2:1. This might be attributable to the liquid contact angle and initial nucleation site (supplementary text). Considering the strongest polar direction [001] is perpendicular to [110] but not to [101], the [101]-oriented films were preferable to show a stronger out-of-plane piezoelectricity. The film thickness could be tuned by the initial volume of the liquid layer. However, because more solution was involved, the diffusion and separation of PVA became more challenging and thus jeopardized the formation of the sandwich structure. The film cross section became irregular, and more random particles of glycine appeared when the film thickness increased to 50 μm and greater (figs. S11 and S12). Accordingly, α-glycine started to appear (fig. S13). Both ratio and thickness relationships confirmed the essential role of the sandwich structure for the formation of piezoelectric γ-glycine films.

The rigid structure of glycine crystals makes it challenging to use in flexible systems. The sandwich structure with two soft PVA encapsulating layers largely improves its flexibility and mechanical integrity. The elastic behaviors of films made from different glycine-to-PVA ratios (30 μm in thickness) and with negligible water content (fig. S14) were examined under different mechanical stimuli (fig. S15). As shown by the stress-strain curves in Fig. 2A, films with higher PVA content (glycine-to-PVA ratio ≤2:1) exhibited substantially enhanced stretchability with tensile strains greater than 0.2%, whereas films with a glycine-to-PVA ratio greater than 3 rapidly fractured at tensile strains less than 0.07%. The evolution of internal cavities at higher glycine concentrations (fig. S8F) may be responsible for the increased fragility. Elastic moduli were calculated from the stress-strain curves. For films with a glycine-to-PVA ratio less than 2:1, the moduli all remained at a moderate level of ~4 GPa (Fig. 2B), which was nearly an order of magnitude smaller than pure glycine crystals (~30 GPa). As the ratio rose over 2:1, the modulus jumped substantially and reached 9 GPa at a 5:1 ratio.

We studied the dynamic mechanical responses of these films at different straining frequencies and amplitudes. As shown in Fig. 2C, flexibility remained consistently low under a repeating 0.1% strain at frequencies less than 10 Hz for films with a glycine-to-PVA ratio ≤3:1. This range covers the frequency range of most biomechanical movements (0.5 to 5 Hz). The moduli slightly increased as frequency rose higher than 10 Hz because of the relatively slow recovery leading to a more elastic response. Only the film with the highest glycine content exhibited a rapid breakdown at 1 Hz. Likewise, films with a glycine-to-PVA ratio less than 3 had a stable elastic performance even with strain up to 0.2% (Fig. 2D). The static and dynamic mechanical characterizations together reveal considerably

improved flexibility and stretchability of the sandwiched thin-film structure. In addition to the flexibility gain as a result of the large size-to-thickness ratio of the wafer-scale films, the soft and continuous PVA encapsulation layers could effectively dissipate the mechanical impacts on the fragile glycine crystals. Meanwhile, the compact and uniform glycine crystals seamlessly fused by PVA precipitates also largely minimized the weak or defective spots in the film.

The piezoelectric performance of the glycine-PVA films was first evaluated by measuring the electric output under impulse forces. A 60-mm^2 molybdenum (Mo) layer (100 nm) was deposited on each side of the films to serve as the electrodes. A 30-N impulse force was repeatedly applied to the film surface over an area of 25 mm^2 at a frequency of 3 to 5 Hz. Figure 3A shows a stable piezoelectric voltage output from a 30-μm-thick 2:1 glycine-PVA film. Films with other glycine-to-PVA ratios also exhibited appreciable piezoelectric outputs (Fig. 3B and fig. S16). The peak-to-peak voltage (V_{pp}) of 4.1 V was among the highest of reported piezoelectric biomaterials, such as poly-L-lactide (PLLA) (23, 24) and diphenylalanine peptide (25, 26), and was substantially higher than other glycine-based composites (27). The peak-to-peak short-circuit current (I_{pp}) also reached as high as 360 nA (fig. S17). The V_{pp} also exhibited an excellent linearity [coefficient of determination (R^2) > 99%] with a force from 0.2 to 10 N (fig. S18), confirming the sensitive piezoelectric responses under small impulse forces that were not damped by PVA encapsulation.

The bulk-scale piezoelectric property was further quantified by a d_{33} meter (fig. S19) on films with different glycine-to-PVA ratios (30 μm in thickness; Fig. 3B). The highest d_{33} (~5 to 6 pC/N) was observed from the film with a 2:1 to 3:1 ratio as a result of the uniform polarization alignment across the film (Fig. 3C), where PVA had negligible contribution (fig. S20). These values are superior to most reported bio-organic films such as silk (1.5 pC/N) (12), collagen (2.6 pC/N) (13), chitin (4 pC/N) (28), and cellulose (1.3 pC/N) (18). The initial increase in d_{33} following the glycine ratio could be attributed to the vertical orientation of glycine films shifting from [110] to [101], which exposed a larger portion of the (001) polar surface toward to the out-of-plane direction (figs. S21 and S22). A further increase of the glycine ratio beyond 3:1 reduced both voltage output and d_{33}. Although glycine retained most of the γ phase at higher concentrations, the crystal discontinuity and separation from the PVA encapsulating layers were not favorable for the γ-glycine domain alignment, as evidenced by the nonuniform second-harmonic generation contrasts (fig. S23). Thicker films also exhibited reduced d_{33} owing to the loss of sandwiched structure (fig. S24). Nevertheless, once the aligned γ-glycine was confined by the PVA layers, its piezoelectric performance was stable. The V_{pp} output retained a constant value of ~4.1 V when subjected to more than 10,000 cycles of 30-N impulse force application (Fig. 3D).

To show the wafer-scale uniformity of the piezoelectric property, d_{33} was measured from eight different areas across a 7-cm film. d_{33} values distributed within a narrow range from 4.9 to 5.7 pC/N between spots, evidencing the good wafer-scale uniformity control of this approach (fig. S25). The repeatability was demonstrated by collecting d_{33} data from five films with the same composition and size, all of which were within a range of 4.0 to 7.4 pC/N (fig. S26 and table S1). Because of their low permittivity of 3.8 (fig. S27), the glycine-PVA films had a high piezoelectric voltage coefficient (g_{33} = 157.5 ×

10^{-3} Vm/N; see materials and methods). This value is the same order of magnitude as PVDF, and higher than most piezoelectric ceramics, such as lead zirconate titanate (PZT), $BaTiO_3$, and sodium potassium niobate. The high g_{33} explains the volt-level output from such a small film thickness, suggesting its capability to produce high-voltage signals with an ultrathin and flexible geometry under low mechanical stimuli—a critical feature for biological applications.

Because both PVA and glycine are water soluble, the glycine-PVA films could dissolve into an aqueous solution in as little as 5 min (fig. S28). After being packaged by 30-μm polylactic acid (PLA), a 2:1 glycine-PVA film was placed in a phosphate buffered saline (PBS) solution, and the piezoelectric output was evaluated at different time points. As shown in Fig. 3E, the V_{pp} output remained at a stable ~4.1 V during the first 3 days and then slightly dropped by ~10% on the fourth day. The fifth day witnessed a notable reduction of V_{pp} to ~33% of its original value, and the device completely failed on the sixth day as a result of solution infiltration when an area of the package dissolved (Fig. 3F). The entire device could be completely dissolved in PBS solution in 10 weeks (fig. S29).

Biocompatibility was confirmed by culturing the device with human fibroblast cells (HFCs). Because glycine-PVA is dissolvable in water, the cell viability tests were performed in a Dulbecco's modified Eagle's medium (DMEM) solution with various amounts of glycine-PVA film dissolved inside. Immunofluorescence staining was performed over a 3-day period to examine the cell morphology and proliferation. As shown in Fig. 4A, all HFCs exhibited normal behavior and reached a higher density with a typical filamentous and stretched morphology on days 2 and 3. The cell morphologies, distributions, and densities did not show any significant differences among groups. Quantitative analysis revealed that the cell viabilities at different concentrations all remained at about 100% during the 3-day period, evidencing the noncytotoxic nature of glycine-PVA films (Fig. 4B).

To demonstrate the application potential in biological systems, the piezoelectric performance of PLA-packaged glycine-PVA films was tested in vivo in adult Sprague-Dawley (SD) rats. Devices with a size of 5 mm by 10 mm were implanted under the skin in the thigh and chest areas where substantial biomechanical energy was accessible (Fig. 4C). When the leg was gently stretched at a frequency of ~1 Hz, the embedded device attached to quadriceps femoris muscle produced a consistent V_{pp} of >150 mV (Fig. 4D and movie S4). The device affixed on top of the pectoralis major muscle in the chest generated a stable V_{pp} of >20 mV in response to rat respiration (Fig. 4E). This level of voltage output was comparable to other reported flexible nanogenerators made from high-performance piezoelectric materials, such as PVDF, PLLA, and ZnO implanted at similar locations (29, 30).

In vivo biodegradation and bioresorption were demonstrated by implanting an unpack-aged glycine-PVA device (5 mm by 10 mm) under the skin in the dorsal region of SD rats (left image in Fig. 4F and fig. S30). Small-animal computed tomography (CT) images of the implantation site showed the rectangular device with distinct contrast from the surrounding tissues (middle two images in Fig. 4F). After 1 day of implantation, the device completely disappeared, and no other changes could be observed from the surrounding tissues (right two images in Fig. 4F). Blood tests were conducted during the implantation period to

further confirm the biocompatibility during degradation (Fig. 4G). The implanted device did not induce any significant change in red blood cells, confirming no signs of anemia. The normal white blood cell level suggested that there was no inflammation in the body due to implantation and degradation. Although a slight increase in platelets was observed at 1 week after implantation, they quickly dropped back to their original level in week 2. This short abnormal level (still within the normal range) was typically due to postsurgery coagulation. These results suggest that the piezoelectric glycine-PVA film can safely serve as an implantable material building block that performs electromechanical functions.

We developed a scalable approach for growing flexible piezoelectric glycine thin films by evaporating solvent from a glycine-PVA mixture solution. The as-received film automatically assembled into a PVA-glycine-PVA sandwich heterostructure as it salted out. Strong hydrogen bonding between the O atoms in glycine and –OH on PVA chains is responsible for the nucleation and growth of the piezoelectric γ-glycine and alignment of the domain orientation. The sandwiched heterostructure was critical for introducing a long-range self-aligned PVA-glycine interaction, leading to strong macroscopic piezoelectricity. Such a heterostructure also substantially improved the flexibility and mechanical integrity, converting rigid glycine crystals into a flexible thin film. Films with appropriate glycine-to-PVA ratios exhibited impressive piezoelectric responses with a g_{33} of 157.5×10^{-3} Vm/N, which is comparable to commercial piezoelectric soft materials, such as PVDF. The biomaterial nature of the film's components allowed it to be used as a bio-compatible and fully biodegradable building block, providing an outstanding piezoelectric function. This work offers a scalable and simple solution for creating high-performance piezoelectric biomaterials applicable for the development of transient implantable electromechanical devices.

Supplementary Material

Refer to Web version on PubMed Central for supplementary material.

ACKNOWLEDGMENTS

Funding:

This work is supported, in part, by the National Institutes of Health under award numbers R01EB021336 and R21EB027857. The small animal imaging facility is supported by the National Institutes of Health under award number P30CA014520. The content is solely the responsibility of the authors and does not necessarily represent the official views of the National Institutes of Health.

Data and materials availability:

All data are available in the manuscript or the supplementary materials.

REFERENCES AND NOTES

1. Shamos MH, Lavine LS, Nature 213, 267–269 (1967). [PubMed: 6030604]
2. Anderson JC, Eriksson C, Nature 227, 491–492 (1970). [PubMed: 5428466]
3. Li J, Long Y, Yang F, Wang X, Curr. Opin. Solid State Mater. Sci 24, 100806 (2020). [PubMed: 32313430]

4. Dagdeviren C et al., Nat. Biomed. Eng 1, 807–817 (2017). [PubMed: 31015594]
5. Lee HS et al., Adv. Funct. Mater 24, 6914–6921 (2014).
6. Hu H et al., Sci. Adv 4, eaar3979 (2018). [PubMed: 29740603]
7. Masmanidis SC et al., Science 317, 780–783 (2007). [PubMed: 17690289]
8. Wang X, Song J, Liu J, Wang ZLJS, Science 316, 102–105 (2007). [PubMed: 17412957]
9. Someya T, Bao Z, Malliaras GG, Nature 540, 379–385 (2016). [PubMed: 27974769]
10. Li C et al., Nat. Rev. Mater 5, 61–81 (2020).
11. Fukada E, J. Phys. Soc. Jpn 11, 1301A (1956).
12. Yucel T, Cebe P, Kaplan DL, Adv. Funct. Mater 21, 779–785 (2011). [PubMed: 23335872]
13. Denning D et al., ACS Biomater. Sci. Eng 3, 929–935 (2017). [PubMed: 33429565]
14. Zhou Z, Qian D, Minary-Jolandan M, ACS Biomater. Sci. Eng2, 929–936 (2016). [PubMed: 33429502]
15. Guerin S et al., Nat. Mater 17, 180–186 (2018). [PubMed: 29200197]
16. Guerin S et al., Phys. Rev. Lett 122, 047701 (2019). [PubMed: 30768312]
17. Fukada E, Sasaki S, J. Polym. Sci. Polym. Phys. Ed 12, 1845–1847 (1975).
18. García Y, Ruiz-Blanco YB, Marrero-Ponce Y, Sotomayor-Torres CM, Sci. Rep 6, 34616 (2016). [PubMed: 27708364]
19. Lee BY et al., Nat. Nanotechnol 7, 351–356 (2012). [PubMed: 22581406]
20. Iitaka Y, Acta Crystallogr 14, 1–10 (1961).
21. Tesei G, Paradossi G, Chiessi E, J. Phys. Chem. B 118, 6946–6955 (2014). [PubMed: 24877893]
22. De Feijter JA, Benjamins J, J. Colloid Interface Sci 81, 91–107 (1981).
23. Curry EJ et al., Proc. Natl. Acad. Sci. U.S.A 115, 909–914 (2018). [PubMed: 29339509]
24. Curry EJ et al., Proc. Natl. Acad. Sci. U.S.A 117, 214–220 (2020). [PubMed: 31871178]
25. Kory J, Steve K, Vu N, Ying W, Rusen Y, Nano Energy 51,317–323 (2018).
26. Nguyen V, Zhu R, Jenkins K, Yang R, Nat. Commun 7, 13566 (2016). [PubMed: 27857133]
27. Hosseini ES, Manjakkal L, Shakthivel D, Dahiya R, ACS Appl. Mater. Interfaces 12, 9008–9016 (2020). [PubMed: 32011853]
28. Kim K et al., Nano Energy 48, 275–283 (2018).
29. Yu Y et al., Nano Energy 27, 275–281 (2016). [PubMed: 28626624]
30. Li Z, Zhu G, Yang R, Wang AC, Wang ZL, Adv. Mater 22, 2534–2537 (2010). [PubMed: 20446305]

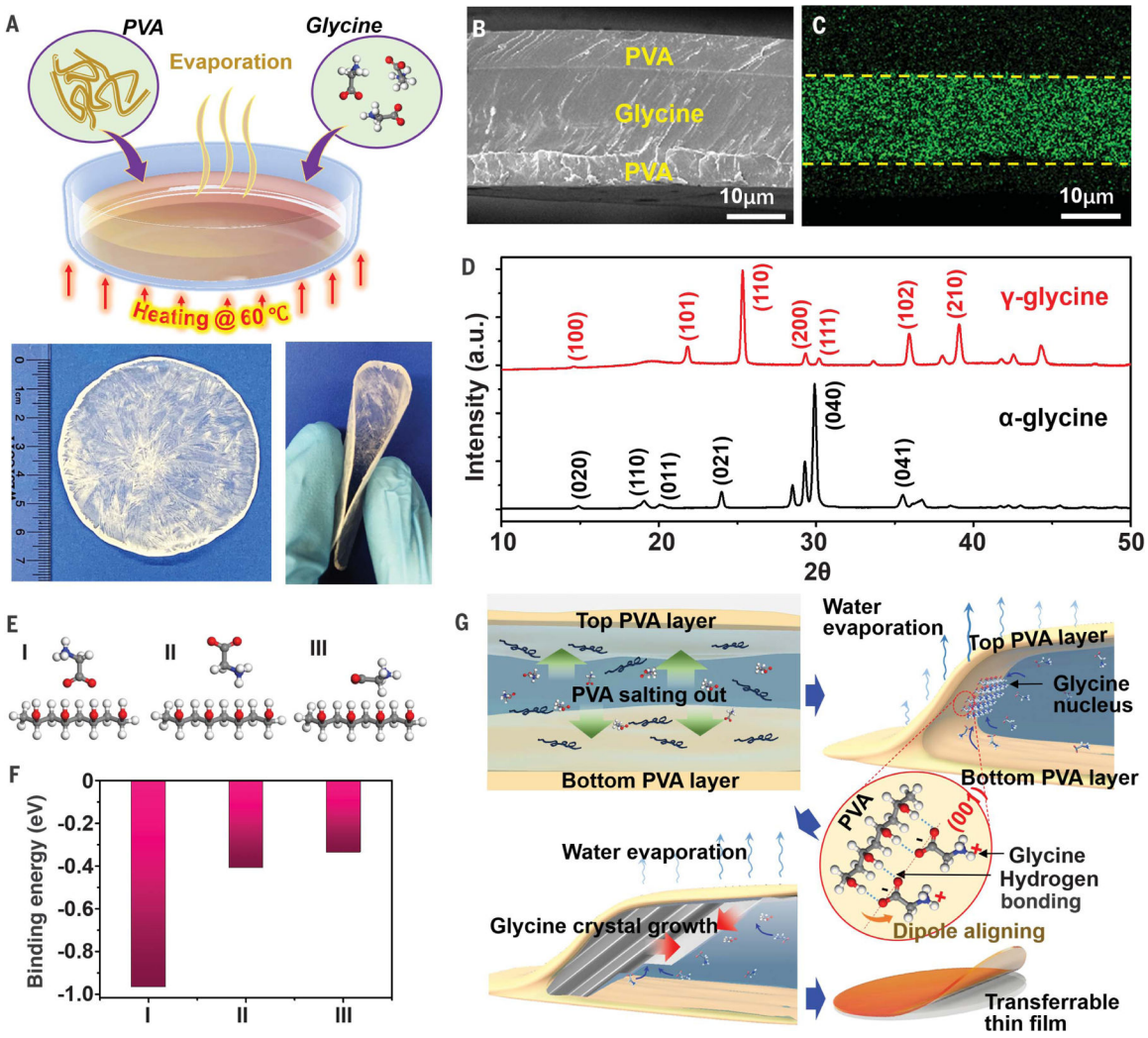

Fig. 1. Synthesis and growth mechanism of piezoelectric glycine-PVA films.

(**A**) Schematic synthesis approach of piezoelectric glycine-PVA films over a large area. Bottom images are digital photographs of a wafer-sized as-grown film (left) and largely curved film showing the flexibility (right). (**B**) Cross-sectional SEM image of a sandwich-structured film. (**C**) Corresponding EDS map of N, confirming that the center layer is glycine. (**D**) XRD spectra of as-prepared glycine-PVA films (red) and pure glycine prepared by the same method (black). (**E**) Schematics of three possible ways for glycine molecules to bind with PVA chains. (**F**) DFT-calculated binding energies for the three binding situations shown in (E). (**G**) Schematic crystallization process of glycine-PVA sandwich thin films. The inset shows the orientation alignment of glycine molecules at the PVA surface during nucleation, leading to long-range crystal alignment.

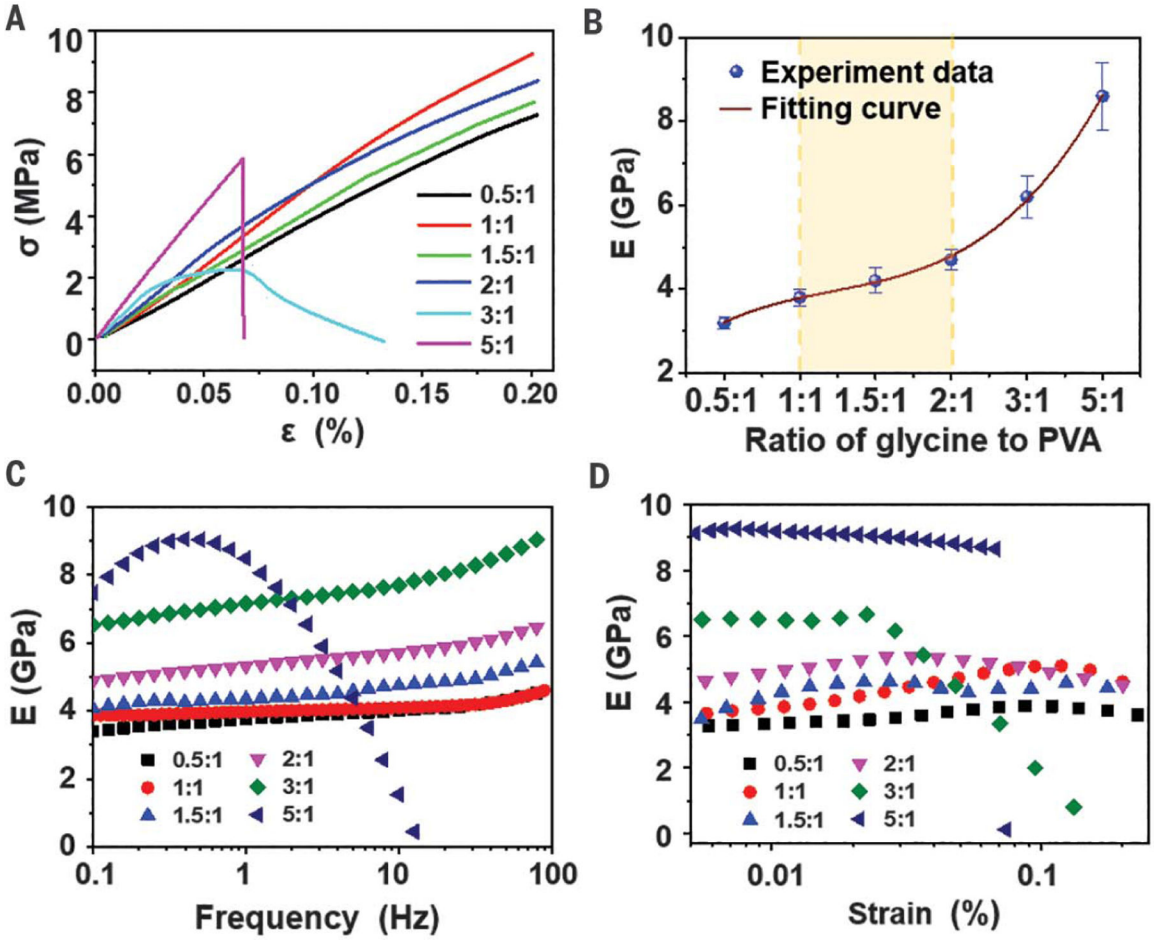

Fig. 2. Mechanical properties of glycine-PVA films.

(**A**) Stress-strain curves of as-prepared films with different composition ratios. σ, stress; ε, strain. (**B**) Elastic moduli of the glycine-PVA films calculated from the stress-strain curves in (A). The yellow shaded region represents the optimal film composition that offered both low moduli and appreciable piezoelectric performance. E, elastic modulus. (**C**) Dynamic mechanical analysis of as-prepared glycine-PVA films in the frequency sweep mode from 0.1 to 100 Hz at a constant strain of 0.1%. (**D**) Dynamic mechanical analysis of as-prepared glycine-PVA films in the strain sweep mode from 0.005 to 0.2% strain at a constant frequency of 1 Hz.

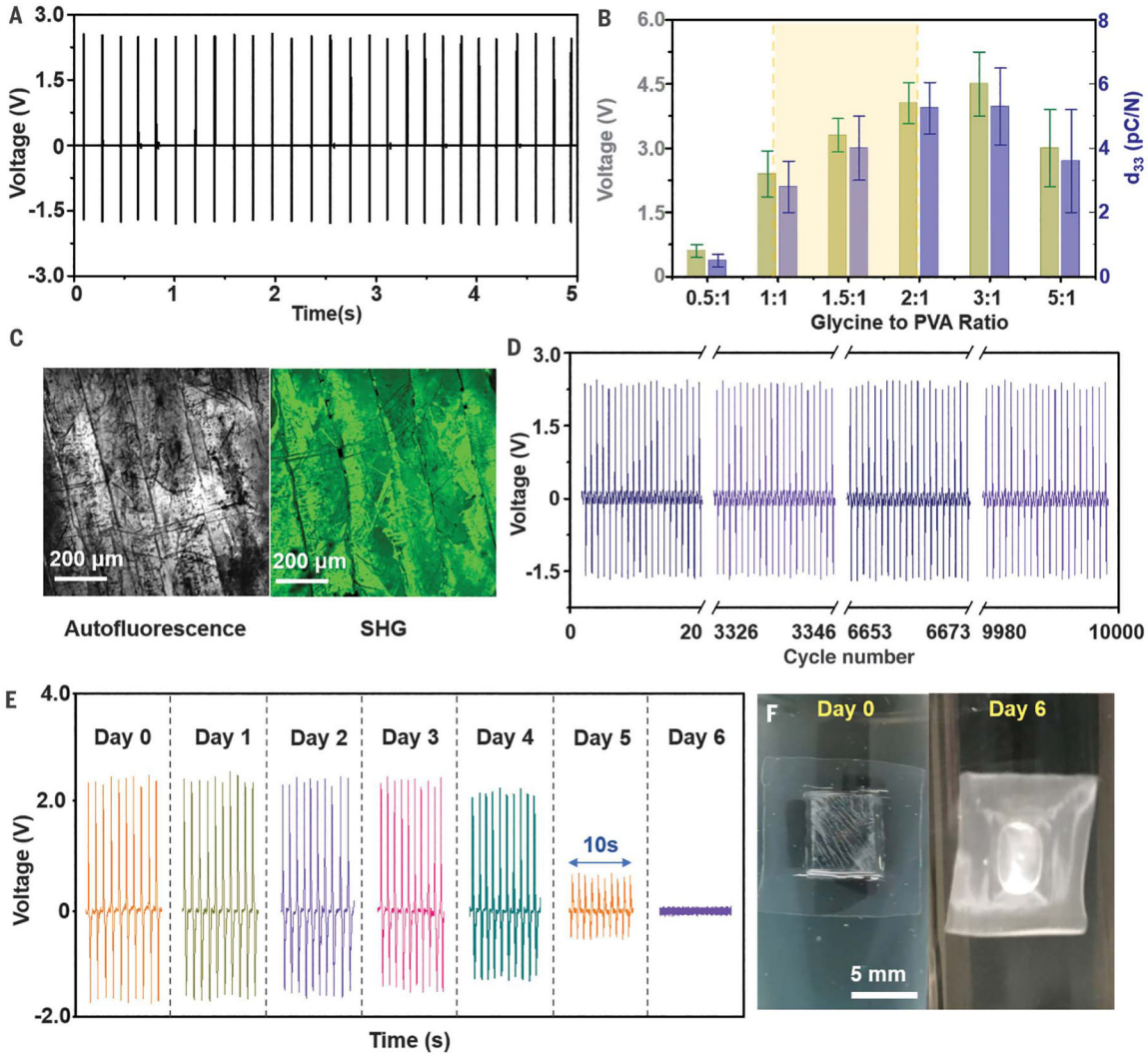

Fig. 3. Piezoelectric property of glycine-PVA films.

(**A**) Piezoelectric voltage output of glycine-PVA films at a 2:1 ratio measured under a 30-N impulse force. (**B**) Piezoelectric voltage out and d_{33} coefficients measured of glycine-PVA films with different composition ratios. (**C**) Autofluoresence and second-harmonic generation images of a 2:1 glycine-PVA film surface showing uniform polarization contrast. (**D**) Long-term stability of the piezoelectric output tested under continuous 30 N impulse force over 10,000 cycles. (**E**) Time-dependent piezoelectric voltage outputs of a packaged glycine-PVA film after being immersed in PBS buffer solution. (**F**) Infiltration of solution into the package which led to the dissolution of glycine film inside and cease of function.

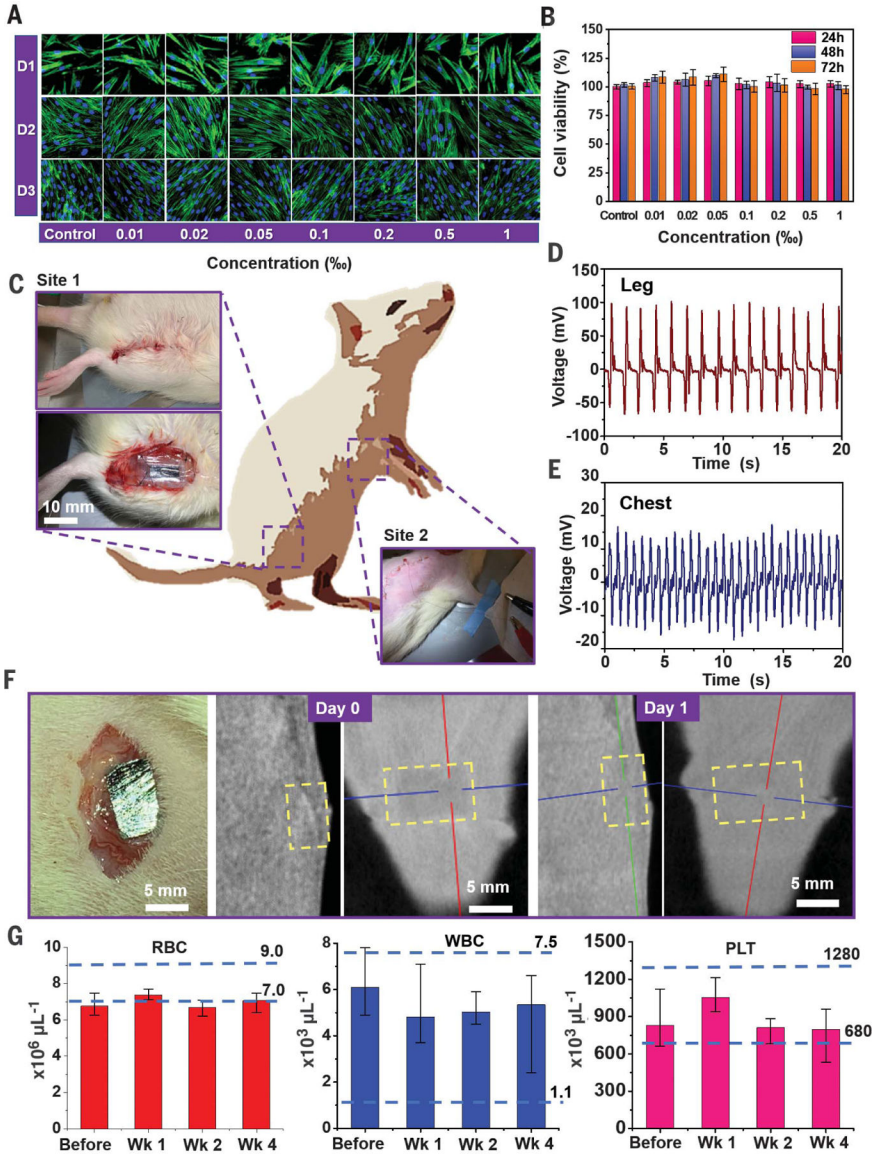

Fig. 4. In vivo piezoelectric performance of packaged glycine-PVA films.

(**A**) Fluorescence microscopy images showing the normal morphology evolution of HFCs cultured in a DM solution with various amounts of PVA-glycine film dissolved inside during a period of 3 days (D1 to D3). Green indicates the cytoskeleton, and blue indicates the nucleus. (**B**) Quantitative cell viability analysis and comparison during a 3-day culturing period. (**C**) Schematic image and digital photographs of the implantations of packaged glycine-PVA films in the thigh and chest areas of SD rats. (**D**) Piezoelectric voltage outputs of the glycine-PVA film implanted on the quadriceps femoris muscle at the thigh area during gentle stretching. (**E**) Piezoelectric voltage outputs of the glycine-PVA film driven by respiration when implanted on the pectoralis major muscle in the chest. (**F**) Observation of the biodegradation of a glycine-PVA film inside a rat body at the subdermal dorsal region. The left image shows the device being implanted; the middle and right images are CT images of the implantation area immediately and 1 day after implantation, respectively.

Yellow boxes mark the location of the implanted film. (**G**) Blood test results during the 4-week implantation period, including red blood cells (RBC; left), white blood cells (WBC, middle), and platelets (PLT, right). Dashed lines indicate the normal range. Error bars represent standard deviation.